

The Impact of Increasing Stratospheric Radiative Damping on the QBO Period

Tiehan Zhou^{1,2}, Kevin DallaSanta^{1,3}, Larissa Nazarenko^{1,2}, Gavin A. Schmidt¹

¹NASA Goddard Institute for Space Studies, New York, NY

²Center for Climate Systems Research, Columbia University, New York, NY

³Universities Space Research Association, Columbia, MD

Correspondence to: Tiehan Zhou (tz2131@columbia.edu)

Abstract. Stratospheric radiative damping increases as atmospheric carbon dioxide concentration rises.

We use the one-dimensional mechanistic models of the QBO to conduct sensitivity experiments and find that when atmospheric carbon dioxide concentration increases, the simulated QBO period shortens due to the enhancing of radiative damping in the stratosphere. This result suggests that increasing stratospheric radiative damping due to rising CO₂ may play a role in determining the QBO period in a warming climate along with wave momentum flux entering the stratosphere and tropical vertical residual velocity, both of which also respond to increasing CO₂.

1. Introduction

The quasi-biennial oscillation (QBO) dominates the variability of the equatorial middle and lower stratosphere and is characterized by a downward propagating zonal wind regime that regularly changes from westerlies to easterlies. The QBO period ranges from 22 to 34 months with its average being slightly longer than 28 months. The QBO not only manifests itself in the equatorial zonal winds, but also leaves an imprint on the temperature in both the tropics and extratropics (Baldwin et al., 2001 and references therein).

The QBO has far-reaching implications for global weather and climate systems. First of all, the QBO exerts a marked influence on the distribution and transport of various chemical constituents such as

27 ozone (O_3) (e.g., Hasebe, 1994), water vapor (H_2O) (e.g., Kawatani et al., 2014), methane (CH_4), nitrous
28 oxide (N_2O), hydrogen fluoride (HF), hydrochloric acid (HCl), odd nitrogen species (NO_y) (e.g.,
29 Zawodny and McCormick, 1991), and volcanic aerosol (Trepte and Hitchman, 1992). Secondly, it is
30 well appreciated that the QBO influences the extratropical circulation in the winter stratosphere, which
31 is commonly known as the Holton–Tan effect (Holton and Tan, 1980; Labitzke, 1982). It has been noted
32 that the effect of the QBO on the extratropical winter stratosphere impacts the severity of stratospheric
33 ozone depletion (e.g., Lait et al., 1989). Furthermore, taking account of the QBO improves the simulation
34 and predictability of the extratropical troposphere (e.g., Marshall and Scaife, 2009). Finally, through its
35 modulation of temperature and vertical wind shear in the vicinity of the tropical tropopause, the QBO
36 influences tropical moist convection (Collimore et al., 2003; Liess and Geller, 2012), the El Niño–
37 Southern Oscillation (ENSO) (Gray et al., 1992; Huang et al., 2012; Hansen et al. 2016), the Hadley
38 circulation (Hitchman and Huesmann, 2009), the tropospheric subtropical jet (Garfinkel and Hartmann,
39 2011a, 2011b), the boreal summer monsoon (Giorgetta et al., 1999), and the Madden-Julian Oscillation
40 (Yoo and Son, 2016). Intriguingly, the QBO is also reported to influence the activities of tropical
41 cyclones (Gray et al., 1984; Ho et al., 2009), albeit this issue is still unsettled (Camargo and Sobel, 2010)
42 and needs further study.

43 Efforts to understand and simulate the QBO have been ongoing ever since its discovery by Ebdon
44 (1960) and Reed et al. (1961). Lindzen and Holton (1968) and Holton and Lindzen (1972) developed
45 the classical theory of the QBO. Namely, as waves propagate upward, they are attenuated by thermal
46 damping, encounter critical levels, and accelerate and decelerate the mean flow, providing momentum
47 sources for both the westerly and easterly phases of the QBO.

48 Holton and Lindzen’s (1972) model (hereafter referred to as HL model) was further simplified by
49 Plumb (1977), the elegance of which made it a standard paradigm for the QBO. In Plumb’s (1977)

50 Boussinesq formulation, the QBO period is inversely dependent upon both the momentum flux and
51 thermal dissipation rate. Hamilton (1981) further highlighted the role of the radiative damping rate on
52 both the realistic vertical structure and the realistic period of the QBO.

92 By adopting higher vertical resolutions and incorporating various gravity wave parameterization
93 schemes, many state-of-the-art climate models have shown the capability to self-consistently simulate
94 the QBO (Scaife et al., 2000; Giorgetta et al., 2002, 2006; Rind et al., 2014, 2020; Geller et al., 2016a;
95 Richter et al., 2020a, 2020b). Given the important implications of the QBO for the global climate system,
96 it is natural to ask how the QBO will change in a warming climate.

97 Giorgetta and Doege (2005) showed a shortening of the QBO period in their doubled CO₂
98 experiments. They reasoned that both the weakening of the tropical upwelling and the prescribed
99 increase of gravity wave sources lead to the reduction of the QBO period in a warming climate. However,
100 most climate models project a strengthening rather than weakening of tropical upwelling in a warmer
101 climate (Butchart et al., 2006; Butchart 2014; Li et al., 2008). Employing a model without any
102 parametrized non-orographic gravity waves, Kawatani et al. (2011) demonstrated that the intensifying
103 tropical upwelling in a warming climate dominates the counteracting effect of enhanced wave fluxes and
104 consequently projected a lengthening of the QBO period. Using fixed sources of parametrized gravity
105 waves, Watanabe and Kawatani (2012) also projected the QBO longer period in a warming climate and
106 pointed out that the lengthening of the QBO is due to the stronger tropical upwelling. Analyzing four
107 Coupled Model Intercomparison Project phase 5 (CMIP5) models that could simulate a reasonable QBO,
108 Kawatani and Hamilton (2013) found that the projected trends of the QBO period were inconsistent in
109 sign. They further investigated the 60-year operational balloon-borne radiosonde observations provided
110 by the Free Berlin University and detected no significant trend in the QBO period. Richter et al. (2020b)
111 investigated the response of the QBO in a doubled and quadrupled CO₂ climate among eleven models

112 that participated in Phase 1 of the Stratospheric-tropospheric Processes And their Role in Climate QBO-
113 initiative (QBOi; Butchart et al., 2018), and found no consensus on how the QBO period would respond
114 to a changing climate. Recently, Butchart et al. (2020) evaluated ten Coupled Model Intercomparison
115 Project phase 6 (CMIP6) models with realistic QBO in two Shared Socioeconomic Pathways (SSPs,
116 Gidden et al., 2019) scenario simulations and surprisingly found that the QBO period shortens in seven
117 of those ten models in both in both SSP3-7.0 and SSP5-8.5 scenarios although only two and three models
118 show a significant shortening trend in the respective scenarios.

119 It is challenging to ascertain the trend of the QBO period in a warming climate. On one hand, a
120 speeding-up of the Brewer-Dobson circulation in a warming climate leads to a lengthening of the QBO
121 period in most climate models. On the other hand, there is a robust increase in the vertical component of
122 the EP flux for both eastward and westward propagating waves (Richter et al., 2020b; Butchart et al.,
123 2020), indicating that the QBO period shortens due to the enhanced wave driving in a warming climate.
124 The competing effects between enhanced wave driving and a faster Brewer-Dobson circulation suggests
125 that trends in the QBO period are likely to be small and difficult to detect due to the large cycle-to-cycle
126 variability that is reproduced by climate models (Butchart et al., 2020). In addition, uncertainty in the
127 representation of the parameterized gravity waves make it more elusive to detect the trend of the QBO
128 period in a warming climate (Schirber et al., 2015; Richter et al., 2020b).

129 Given the fact that the QBO period is influenced by the radiative damping (Plumb 1977; Hamilton
130 1981), a natural question to ask is whether it could play a role on the trend of the QBO in a warming
131 climate. Plass (1956) showed that when the CO₂ concentration is increased from 330 ppmv to 660 ppmv,
132 the cooling rate increases significantly in the middle and upper stratosphere while it is not changed below
133 the 24 km height level. The cooling rate is increased by more than 50% around the 40 km height level
134 (see his Figure 8).

135 It is well-known that enhanced wave fluxes entering the stratosphere and stronger tropical upwelling
 136 individually play a dominant role in determining the trends in the QBO period in a warming climate.
 137 Does the competing effect between them leave some room for increasing stratospheric radiative damping
 138 to exert an influence on the QBO period? In this paper, we use the HL model to isolate the effect of
 139 radiative damping on the QBO period by assuming that the momentum flux entering the stratosphere
 140 doesn't change in our experiments. Observational and modeling studies (Andrews et al., 1987; Kawatani
 141 et al., 2009, 2010, 2011; Richter et al., 2020b; Holt et al., 2020) showed that the wave forcing spectrum
 142 is similar to a discrete two-wave spectrum rather than red-noise or white-noise, all of which are
 143 illustrated in Saravanan (1990). Accordingly, the QBO is indeed sensitive to stratospheric radiative
 144 damping, and the HL model is suitable for us to conduct the sensitivity test.

145 The remainder of this paper is organized as follows. Section 2 investigates the sensitivity of the QBO
 146 period to the radiative damping using HL's original model. Section 3 explores the sensitivity of the QBO
 147 period to the radiative damping using a modified HL model where the semiannual forcing is removed.
 148 Discussion and conclusions are presented in Sections 4 and 5 respectively.

149 150 **2. Sensitivity of the QBO period to enhanced stratospheric radiative damping in the original HL** 151 **model**

152 In the HL model the governing equation of mean flow emerges after the primitive momentum
 153 equation is meridionally averaged over some suitable latitudinal belt over the equator.

$$154 \quad \frac{\partial \bar{u}}{\partial t} = -\frac{1}{\rho_0} \frac{\partial}{\partial z} \left[\sum_i \bar{F}_i \right] + K_z \frac{\partial^2 \bar{u}}{\partial z^2} + G \quad (1)$$

155 where \bar{u} is mean zonal wind, ρ_0 is mean density, \bar{F}_i is the meridionally averaged vertical Eliassen-Palm
 156 flux associated with wave i , the index i refers to the individual waves, K_z is a vertical eddy diffusion
 157 coefficient, t is time, z is altitude, and G is semiannual forcing identical to that specified by HL.

158 The \bar{F}_i are evaluated with Lindzen's (1971) WKB formalism for equatorial waves in shear. When
 159 only infrared cooling acts to damp the waves the formulae for \bar{F}_i are

$$160 \quad \bar{F}_0(z) = A_0 \exp \left(- \int_{17 \text{ km}}^z \frac{\alpha N}{k(c - \bar{u})^2} dz \right) \quad (2)$$

161 for the Kelvin wave, and

$$162 \quad \bar{F}_1(z) = A_1 \exp \left[- \int_{17 \text{ km}}^z \frac{\alpha \beta N}{k^3(c - \bar{u})^3} \left(1 - \frac{k^2(\bar{u} - c)}{\beta} \right) dz \right] \quad (3)$$

163 for the mixed Rossby-gravity wave. As in HL, the wavenumber k , the phase speed c , and A_0 are chosen
 164 to be $2\pi/(40,000 \text{ km})$, 30 m s^{-1} , and $0.04 \text{ m}^2 \text{ s}^{-2} \rho_0(17 \text{ km})$, respectively for the Kelvin wave while
 165 they are equal to $-2\pi/(10,000 \text{ km})$, -30 m s^{-1} , and $-0.04 \text{ m}^2 \text{ s}^{-2} \rho_0(17 \text{ km})$, respectively for the
 166 mixed Rossby-gravity wave. In Eq. (1), $K_z = 0.3 \text{ m}^2 \text{ s}^{-1}$, which is also the same as in HL. In addition,
 167 $\beta = 2\Omega/a$, where Ω is earth's rotation rate, and a is earth's radius. HL's boundary conditions stipulated
 168 that $\bar{u} = 0$ at the lowest model level (17 km) and constrained \bar{u} to vary semiannually at the top level (35
 169 km).

170 In our control run that is used to depict the present-day QBO all the model parameters are identical
 171 to those used by HL in their original simulation. The Brunt-Väisälä frequency

$$172 \quad N = \sqrt{\frac{g}{T_0} \left(\frac{dT_0}{dz} + \frac{g}{c_p} \right)} \quad (4)$$

173 In Eq. (4), g is gravity, T_0 is mean temperature, and c_p is specific heat of dry air at constant pressure.
 174 HL set N in Eq. (4) to $2.16 \times 10^{-2} \text{ s}^{-1}$ with a scale height $H = 6 \text{ km}$. In addition, the Newtonian

Deleted: ing

176 cooling profile in our control run, i.e., $\alpha(z)$ in Eqs. (2) and (3), is also identical to that in the original
177 HL model and depicted in FIG. 1 as the black line. Namely, $\alpha(z)$ in the control run increases from
178 $(21 \text{ day})^{-1}$ at 17 km to $(7 \text{ day})^{-1}$ at 30 km and is kept at $(7 \text{ day})^{-1}$ between 30 km and 35 km. Fels
179 (1985) explicated why this cooling rate is suitable for simulating the QBO on the basis of the scale-
180 dependent effect of radiative damping (Fels 1982). Hamilton (1981) demonstrated that the proper choice
181 of $\alpha(z)$ is crucial in simulating a realistic vertical structure of the QBO.

182 Eq. (1) was integrated for 100 years using the forward-backward scheme (Matsuno, 1966). The
183 vertical resolution was 250 m and identical to that in HL. The time step was 12 hr, i.e., one half of used
184 in HL, because the 24-hr time step resulted in numerical instability in our integration.

185 FIG. 2a shows the time–height section of the monthly averaged mean zonal wind simulated over the
186 first 20 years using the HL model. Both the QBO and the semiannual oscillation (SAO) are conspicuous.
187 The fast Fourier transform (FFT) method is used to calculate the frequency power spectra. In order to
188 more accurately derive the QBO period, the model was run for 100 years to increase the spectral
189 resolution. Frequency–height sections of the power spectral densities (PSD) over zero to the Nyquist
190 frequency, i.e., 0.5 cycle/month, depict two sharp lines (peaks) at $\frac{1}{30}$ and $\frac{1}{6}$ cycle/month, respectively
191 (not shown). In order to better visualize the magnitudes of the PSD, we show two truncated frequency–
192 height sections with FIG. 2b and FIG. 2c highlighting the QBO and the SAO respectively. FIG. 2b shows
193 that the QBO dominates over the model domain. The peak frequency corresponds to the period of 30
194 months. FIG. 2c shows the SAO dominates near the model top due to the fact a semiannual forcing was
195 imposed in the altitudes from 28 to 35 km.

196 It is worth mentioning that the QBO period shown here is longer than 26.5 months reported in the HL
197 paper (see their FIG. 1). Using the HL model parameters, the QBO period simulated by Plumb (1977)
198 was close to three years (refer to his FIG. 8a), which is longer than our simulated QBO period, i.e., 30.0

199 months. Although we could not explain why our simulated QBO period is longer than that simulated by
 200 HL, we found that when the upper boundary condition is changed from $\bar{u} = 14 \sin(\omega_a t)$ and $\omega_a =$
 201 $\frac{2\pi}{180} \text{ day}^{-1}$ used in the HL's original model (refer to their Eqs. (2)) to $\frac{\partial \bar{u}}{\partial z} = 0$ used in Plumb (1977), the
 202 simulated QBO period becomes 34.3 month (figure not shown). In other words, when we adopted the
 203 stress-free upper boundary condition as in Plumb (1977), our simulated QBO period is comparable to
 204 that simulated by him, which lends credence to our reconstruction of the HL model.

205 As mentioned in Section 1, when the atmospheric carbon dioxide concentration is doubled the cooling
 206 rate increases significantly in the middle and upper stratosphere while it is not changed below the 24 km
 207 height level. The cooling rate is increased by more than 50% around the 40 km height level (Plass, 1956).

208 As implied in Dickinson (1973), his estimated cooling coefficient below the 0.2 hPa level is
 209 approxamtedly proportional to his estimated cooling rate and is not sensitive to the chosen temperature
 210 profile. In other words, the relative increase in the cooling coefficient is roughly equal to the relative
 211 increase in the cooling as the CO₂ concentration is doubled. Accordingly, the Newtonian cooling profile

212 in our experimental run, i.e., $\alpha(z)$ in Eqs. (2) and (3), is specified in FIG. 1 as the red line. Namely, $\alpha(z)$
 213 in the experimental run increases from $(21 \text{ day})^{-1}$ at 17 km to $\frac{9}{91} \text{ day}^{-1}$ at 24 km, which is identical to
 214 that in the control run from 17 km to 24 km. We increased $\alpha(z)$ in the experimental run between 30 km
 215 and 35 km by 30% relative to that in the control run. In other words, $\alpha(z)$ is kept at $\frac{1.3}{7} \text{ day}^{-1}$ between

216 30 km and 35 km in the experimental run. This percentage increase of 30% in $\alpha(z)$ for the doubled CO₂
 217 above 30 km shown in FIG. 1 is somewhat less than that implied in the Figure 8 of Plass (1956), because
 218 we would like our estimated relative increase in $\alpha(z)$ to err on the conservative side given the inherent
 219 uncertainties mentioned by him. Between 24 km and 30 km, $\alpha(z)$ in the experimental run is formulated
 220 linearly with height from $\frac{9}{91} \text{ day}^{-1}$ at 24 km to at $\frac{1.3}{7} \text{ day}^{-1}$ at 30 km.

Deleted: The

Deleted: comparable to

Deleted: in his Figure 8

FIG. 3a shows the time–height section of the monthly averaged mean zonal wind simulated over the first 20 years for the doubled CO₂ run, where the increased $\alpha(z)$ depicted as the red line in FIG. 1 was employed while all other parameters are identical to those in the control run. Obviously, the QBO dominates below 28 km while the semiannual oscillation (SAO) dominates above 31 km. Like FIG. 2b and FIG. 2c, we only show two truncated frequency–height sections with FIG. 3b highlighting the QBO and FIG. 3c highlighting the SAO. FIG. 3b also shows that the QBO dominates over the model domain. The peak frequency corresponds to the period of 27.9 months. FIG. 3c shows the SAO dominates near the model top due to the same imposed semiannual forcing as that in the control run.

In summary, using the original HL model we found that the increased radiative damping due to the doubling of CO₂ shortens the QBO period by 7% (i.e., from 30 months to 27.9 months).

3. Sensitivity of the QBO period to enhanced stratospheric radiative damping in the HL model without the semiannual forcing

HL pointed out that the imposed semiannual oscillation was not essential for their QBO theory. Applying $\frac{\partial \bar{u}}{\partial z} = 0$ as the upper boundary condition, Plumb (1977) showed a simulated QBO without resorting to the semiannual momentum source (refer to his FIG. 8b). In the following control run, all parameters are identical to those used in the previous control run in Section 2 except that G in Eq. (1) is set to zero with $\frac{\partial \bar{u}}{\partial z}$ also being set to zero at $z = 35$ km. Hereafter we refer to it as the Plumb model¹. FIG. 4a shows the time–height section of the monthly averaged mean zonal wind simulated over the first 20 years using the Plumb model. As expected, the QBO emerges without any trace of SAO since $G = 0$ in Eq. (1). FIG. 4b shows that the QBO dominates over the whole model domain. The peak frequency

Deleted: In order to properly investigate the sensitivity of the QBO period to enhanced stratospheric radiative damping in response to the doubled CO₂, it is worth mentioning that both α and N in Eqs. (2) and (3) change with increasing CO₂. Richter et al. (2020b) showed that N^2 would be decreased by ~5% in the stratosphere when CO₂ is doubled (refer to their Figure 2c). Accordingly, the Brunt-Väisälä frequency in the following experimental run, i.e., N in Eqs. (2) and (3), was decreased by ~2.5% compared with that in the previous control run.

Deleted: .

Deleted: 28.6

Deleted: 4.7%

¹ Strictly speaking, it is the HL model modified by Plumb (1977). In this paper, we don't use his eponymous model, i.e., the simplest possible model of the QBO, where Boussinesq fluids with uniform mean density were employed, because the HL model and its variant are considerably more realistic.

corresponds to the period of 37.5 months, which is comparable to that simulated by Plumb (1977) shown in his FIG. 8b. Apparently, the QBO period from the Plumb model, i.e., 37.5 months shown in FIG. 4b, is longer than that from the HL model, i.e., 30.0 months shown in FIG. 2b. This is partly because the additional forcing G in Eq. (1) was removed in the Plumb model.

In the following experimental run, all parameters are identical to those used in the previous experimental run in Section 2 except that G in Eq. (1) is set to zero with $\frac{\partial \bar{u}}{\partial z}$ also being set to zero at $z = 35$ km. In other words, the following experimental run using the Plumb model employed the same parameters as the afore-mentioned control run using the Plumb model ~~except that, the increased $\alpha(z)$~~ shown as the red line in FIG. 1 was used in the following experimental run while $\alpha(z)$ shown as the black line in FIG. 1 was used in the above control run. FIG. 5a shows the time–height section of the monthly averaged mean zonal wind simulated over the first 20 years for the doubled CO₂ run. It is natural that only the QBO emerges. A comparison of FIG. 4a and FIG. 5a shows that the QBO period shortens when the infrared damping increases in response to the doubled CO₂. FIG. 5b shows that the QBO dominates over the whole model domain. The peak frequency corresponds to the period of 31.6 months.

Using the Plumb model, we found that the increased radiative damping due to the doubling of CO₂ shortens the QBO period by 15.7%.

4. Discussion

The semiannual forcing, G in Eq. (1), in the HL model is imposed rather than results from the wave–flow interaction. In other words, G in Eq. (1) is independent of mean flow, and is specified as $G = 0$ for $z \leq 28$ km, and $G = \omega_{sa} \bar{u}_{sa}$ for $z > 28$ km

Deleted: with the following two exceptions.

Deleted: Namely,

Deleted: In addition, the Brunt-Väisälä frequency, i.e., N in Eqs. (2) and (3), was decreased by 2.5% in the following experimental run compared with that in the above control run.

285 where $\bar{u}_{sa} = 2(z - 28\text{km}) \text{ m s}^{-1} \text{ km}^{-1} \sin(\omega_{sa} t)$ and $\omega_{sa} = \frac{2\pi}{180} \text{ day}^{-1} \approx 4 \times 10^{-7} \text{ s}^{-1}$ (refer to
 286 Eqs. (2) in HL). Therefore, we have $\frac{\partial^2 \bar{u}_{sa}}{\partial z^2} = 0$ in the HL original model. We furthermore decompose \bar{u}
 287 into two components: \bar{u}_{QBO} and \bar{u}_{sa} . Combining Eq. (1), the decomposition of \bar{u} as $\bar{u} = \bar{u}_{QBO} + \bar{u}_{sa}$,
 288 the above-mentioned $\frac{\partial^2 \bar{u}_{sa}}{\partial z^2} = 0$, and $G = \omega_{sa} \bar{u}_{sa} = \frac{\partial \bar{u}_{sa}}{\partial t}$ for $z > 28 \text{ km}$, yields

$$289 \quad \frac{\partial \bar{u}_{QBO}}{\partial t} = -\frac{1}{\rho_0} \frac{\partial}{\partial z} \left[\sum_{i=0}^1 \bar{F}_i \right] + K_z \frac{\partial^2 \bar{u}_{QBO}}{\partial z^2} \quad (5)$$

290 for $z > 28 \text{ km}$.

291 Dunkerton (1997) showed that in the presence of tropical upwelling it was gravity waves rather than
 292 large-scale Kelvin and mixed Rossby-gravity waves that contributed the bulk of QBO forcing.
 293 Consequently, Geller et al. (2016a, 2016b) pointed out that enough gravity wave momentum flux is
 294 required to model the QBO in a self-consistent manner in climate models and that the magnitude of the
 295 subgrid-scale gravity wave momentum flux plays a crucial role in determining the QBO period. Since
 296 there is no tropical upwelling in either the HL model or the Plumb model, and the semiannual forcing,
 297 G , is dependent on neither \bar{u} in Eq. (1) nor \bar{u}_{QBO} in Eq. (5), it is natural that planetary-scale Kelvin and
 298 mixed Rossby-gravity waves largely determine the QBO periods shown in Sections 2 and 3 due to the
 299 fact that G only exerts a weak influence on the planetary wave forcing, i.e., $-\frac{1}{\rho_0} \frac{\partial}{\partial z} [\sum_{i=0}^1 \bar{F}_i]$ in Eqs. (1)
 300 and (5). We conducted another sensitivity test where all parameters are identical to those in the HL model
 301 except that G in both the control and experimental runs is twice as large as that used by HL. As the
 302 radiative damping profile changes from the black line to the red line above 24 km shown in FIG. 1, our
 303 simulated QBO period decreases from ~~28.6~~ months to ~~27.3~~ months (figures not shown). This smaller
 304 percentage decrease of ~~4.5%~~ is not unexpected because the unrealistically larger G that is independent
 305 of \bar{u} makes the model atmosphere less sensitive to the changes in the radiative damping.

Deleted: meanwhile the Brunt-Väisälä frequency is decreased by 2.5% in the experimental run

Deleted: 28.4

Deleted: 27.6

Deleted: 2.8%

311 We further conducted two sensitivity tests where all parameters are identical to those in the HL model
 312 except that G in the first test is half as large as that used by HL and is equal to zero in the second test.
 313 Surprisingly, as the radiative damping profile changes from the black line to the red line above 24 km
 314 shown in FIG. 1, our simulated QBO periods decreases from 30.0 months to 28.6 months both for G
 315 being decreased by 50% and for $G = 0$ (figures not shown). This 4.7% decrease in the QBO period is
 316 somewhat smaller than the 7% reduction obtained from the sensitivity test presented in Section 2 when
 317 G is the same as that used by HL. It is surprising because the model atmosphere is expected to be more
 318 sensitive to the changes in the radiative damping as G , which is independent of \bar{u} , becomes smaller and
 319 smaller. Note that when our control runs adopt the black radiative damping profile shown in FIG. 1 the
 320 simulated QBO periods are not sensitive to the imposed semiannual forcing provided that G does not
 321 exceed the values employed by HL. Similarly, when our experimental runs adopt the red radiative
 322 damping profile above 24 km shown in FIG. 1 the simulated QBO periods are also not sensitive to the
 323 imposed semiannual forcing provided that G does not exceed 50% of the values adopted in HL. The
 324 question naturally arises: what is responsible for this unphysical behavior?

325 Plumb (1977) pointed out that the upper boundary in HL was undesirably low and implied that raising
 326 the lid to an additional 50% would be adequate for the robustness in his model. Here, we carry out a
 327 series of sensitivity tests by raising the model lid gradually from 35 km to 55 km with the one-kilometer
 328 increment. we will demonstrate how the behavior of the HL model with $G = 0$ converges with that of
 329 the Plumb model. The modified HL model, i.e., the HL model with $G = 0$ is identical to the Plumb
 330 model except that the former has the no-slip upper boundary condition while the latter has the stress-free
 331 upper boundary condition. Both models share the same governing equation (5). Note that we set the
 332 radiative damping rate above the 35 km level to its value at the 35 km level shown in FIG. 1.

Deleted: while the Brunt-Väisälä frequency is decreased by 2.5% in the experimental runs

Deleted: identical to

336 For the radiative damping profile corresponding to the reference CO₂, FIG. 6 shows that when the
 337 model lid is placed at the 35 km level the simulated QBO period of 30.0 months with the no-slip upper
 338 boundary condition (solid black line) is apparently shorter than that of 37.5 months with the stress-free
 339 upper boundary condition (dashed black line). FIG. 6 also shows that as the model lid is raised
 340 incrementally from the 35 km level to the 46 km level, the discrepancies between the simulated QBO
 341 periods due to the different upper boundary conditions decrease monotonically. No matter whether we
 342 adopt the no-slip or stress-free upper boundary condition, the simulated QBO period is 32.4 months for
 343 the reference radiative damping profile provided that the model top is at or above the 46 km level.

344 Similarly, for the radiative damping profile corresponding to the doubled CO₂, FIG. 6 demonstrates
 345 that when the model lid is placed at the 35 km level the simulated QBO period of 27.9 months with the
 346 no-slip upper boundary condition (solid red line) is obviously shorter than that of 31.6 months with the
 347 stress-free upper boundary condition (dashed red line). FIG. 6 also exhibits that as the model lid is raised
 348 gradually from the 35 km level to the 40 km level, the discrepancies between the simulated QBO periods
 349 due to the different upper boundary conditions decrease monotonically. No matter whether we adopt the
 350 no-slip or stress-free upper boundary condition, the simulated QBO period for the enhanced infrared
 351 cooling due to the doubled CO₂ is 30.0 months provided that the model top is at or above the 40 km level.
 352 It is apparent that the required model top is lower when the radiative damping is augmented due to the
 353 doubling of CO₂ because the planetary waves dissipate more steeply with height in presence of the
 354 enhanced infrared cooling rates.

355 FIG. 6 suggests that when the model lid is sufficiently high the QBO period in response to the
 356 enhanced radiative damping due to the increasing CO₂ will decrease from 32.4 to 30.0 months. This 7.4%
 357 decrease in the QBO period is independent of the upper boundary condition. Plass (1956) indicated that
 358 the probable error of the cooling rate was about 10 per cent below 20 km, increasing to 30 per cent at 50

Deleted: 30.0 months when the model lid is placed at 35 or 36 km level; 30.8 months when the model lid is placed at 37, 38, or 39 km level; 31.6 months when the model lid is placed between the 40 and 45 km levels; 32.4 months when the model lid is placed at or above the 46 km level while the simulated QBO period

Deleted: in FIG. 6

Deleted: decreases from 37.5 to 35.5 months as the model lid is raised from the 35 to 36 km level

Deleted: ;

Deleted: continues decreasing to 34.3 and 33.3 months as the model lid is raised to 37 and 38 km level, respectively; is kept at 33.3 months when the model lid is placed between the 38 and 41 km levels; and it further decreases to 32.4 months when the model lid is placed at or above the 42 km level.

Deleted: shows

Deleted: that the simulated QBO period with the no-slip upper boundary condition (solid red line) is 28.6 months when the model lid is placed at 35 km level; 29.3 months when the model lid is placed at 36, 37, or 38 km level; 30.0 months when the model lid is placed at or above the 39 km level while the simulated QBO period with the stress-free upper boundary condition (dashed red line in FIG. 6) decreases from 31.6 to 30.8 months as the model lid is raised from the 35 to 36 km level; and is kept at 30.0 months when the model lid is placed at or above to 37 km level.

Deleted: 39

Deleted: ed

Deleted: demonstrates

Deleted: the response of

390 km and that the relative differences between the various curves should be considerably more accurate
391 than their magnitude. In other words, the relative differences between the various cooling rates calculated
392 by Plass (1956) should be considerably smaller 30%. Using the HL model with its top at the 48 km level,
393 we further conducted two experiments by adopting $G = 0$ in Eq. (1) and increasing the radiative
394 damping corresponding to the doubled CO_2 between 30 km and 48 km by $30\% - 30\% * 30\% = 21\%$
395 and $30\% + 30\% * 30\% = 39\%$ respectively relative to that in the control run. The simulated QBO
396 periods are 30.8 and 29.3 months respectively. Therefore, when the model lid is sufficiently high the
397 QBO period in response to the enhanced radiative damping due to the doubled CO_2 will decrease by
398 approximately $7.4\% \pm 2.5\%$.

399 Note that N , the Brunt-Väisälä frequency, in Eqs. (2) and (3) also changes with increasing CO_2 .
400 Richter et al. (2020b) showed that N^2 would be decreased by $\sim 5\%$ in the stratosphere when CO_2 is
401 doubled (refer to their Figure 2c). We used the HL model to conduct a sensitivity test by adopting $G = 0$
402 in Eq. (1) with the radiative damping profile corresponding to the doubled CO_2 and the top of the models
403 at the 48 km level. The rest of parameters in this sensitivity test are identical to those in all the previous
404 runs except that the Brunt-Väisälä frequency in this experimental run was 2.5% smaller than that in the
405 control run. The models were run for 1000 years to further increase the spectral resolution. We found
406 that when the Brunt-Väisälä frequency was decreased by 2.5%, the simulated QBO period was slightly
407 lengthened from 30 months to 30.2 months (figure not shown). In other words, the impact of decreasing
408 stratospheric buoyancy frequency on the QBO Period is marginal.

409 Analyzing eleven CCMI-1 REF-C2 climate-chemistry simulations, Eichinger and Šácha (2020)
410 showed that the scale height in the stratosphere decreases by 2.3% per century. Accordingly, we used
411 the HL model to conduct another sensitivity test by adopting $G = 0$ in Eq. (1) with the radiative damping
412 profile corresponding to the doubled CO_2 and the top of the models at the 48 km level. The rest of

413 parameters in this sensitivity test are identical to those in all the previous control runs except that the
414 scale height in this experimental run was 2.3% smaller than that in the control run. The model was also
415 run for 1000 years for the sake of higher spectral resolution. We found that when the scale height was
416 decreased by 2.3%, the simulated QBO period was also shortened by about 2.3%, i.e., from 30 months
417 to 29.3 months (figure not shown). Apparently, the shortening of the QBO period due to the warming
418 climate is ascribed less to the shrinkage of the scale height in the stratosphere than to the enhancing of
419 the stratospheric radiative damping. Together, the shrinking scale height and the increasing radiative
420 damping shorten the QBO period by about 9.6%.

422 5. Conclusions

423 Plumb (1977) envisioned that stratospheric climate change would give rise to long-term changes in
424 the QBO period due to changes in radiative damping and the Brunt-Väisälä frequency. Using one-
425 dimensional (1D) models we found that the enhanced radiative damping arising from the doubling of
426 CO₂ leads to the shortening of the QBO period by about $7.4\% \pm 2.5\%$ provided that the model top is
427 higher than the 46 km level. Furthermore, when we incorporated both the 2.3% shrinkage of the scale
428 height and the enhanced radiative damping, the QBO period is shortened by about 9.6%. In addition, the
429 impact of decreasing stratospheric buoyancy frequency on the QBO Period is marginal. Those models
430 include neither gravity waves nor tropical upwelling and assume that there are no changes in wave fluxes
431 entering the equatorial stratosphere.

432 From a comprehensive model perspective, Richter et al. (2020b) showed that the changes in period
433 of the QBO in warming climate simulations varied quite significantly among these models. Some models
434 projected longer mean periods and some shorter mean periods for the QBO in a future warmer climate.

435 They argue that uncertainty in the representation of the parameterized gravity waves is the most likely
436 cause of the spread among the QBOi models in the QBO's response to climate change.

437 In addition, CO₂ increases in the NASA Goddard Institute for Space Studies Model E2.2-AP (Rind
438 et al. 2020) lead to a decrease of both QBO period and QBO amplitude (DallaSanta et al., in prep.). The
439 period decrease is associated with increases in lower stratospheric momentum fluxes (related to
440 parameterized convection), a finding consistent with Geller et al. (2016a, 2016b) and Richter et al.
441 (2020b). The amplitude decrease is associated with a strengthened residual mean circulation, also
442 consistent with the literature, although the vertical structure of the circulation response is nontrivial. It
443 is worth mentioning that horizontal momentum flux divergences could also play an important role in
444 weakening the QBO (Match and Fueglistaler, 2019, 2020).

445 Our 1D models only explored how the QBO period responds to the enhancing radiative damping of
446 planetary waves due to the increasing CO₂. In order to investigate how the enhancing radiative damping
447 impacts on gravity waves which play an even more important role in determining the QBO period than
448 planetary waves, high-resolution models such as those used by Kawatani et al. (2011, 2019) are desirable
449 to further our understanding. Ultimately, how the QBO period changes in response to the increasing CO₂
450 will be determined by the combined effects of the strengthening of tropical upwelling, the increasing of
451 wave fluxes entering the equatorial stratosphere, and the enhancing of radiative damping, which warrants
452 further research.

453
454 **Acknowledgements:** Climate modeling at GISS is supported by the NASA Modeling, Analysis and
455 Prediction program, and resources supporting this work were provided by the NASA High-End
456 Computing (HEC) Program through the NASA Center for Climate Simulation (NCCS) at Goddard
457 Space Flight Center. KD acknowledges support from the NASA Postdoctoral Program. The authors
458 also acknowledge very useful discussions with Drs. Geller and Clara Orbe.

459 **References**

- 460 Andrews, D. G., Holton, J. R., and Leovy, C. B.: Middle Atmosphere Dynamics, Academic Press, 489
 461 pp, 1987.
- 462 Baldwin, M. P., Gray, L. J., Dunkerton, T. J., Hamilton, K., Haynes, P. H., Randel, W. J., Holton, J. R.,
 463 Alexander, M. J., Hirota, I., Horinouchi, T., Jones, D. B. A., Kinnnersley, J. S., Marquardt, C., Sato,
 464 K., and Takahashi, M.: The Quasi-biennial oscillation, *Rev. Geophys.*, 39, 179–229,
 465 <https://doi.org/10.1029/1999RG000073>, 2001.
- 466 Butchart, N.: The Brewer-Dobson circulation, *Rev. Geophys.*, 52, 157–
 467 184, <https://doi.org/10.1002/2013RG000448>, 2014.
- 468 Butchart, N., Scaife, A. A., Bourqui, M., Grandpré, J., Hare, S. H., Kettleborough, J., Langematz, U.,
 469 Manzini, E., Sassi, F., Shibata, K., Shindell, D. and Sigmond, M.: Simulations of anthropogenic
 470 change in the strength of the Brewer–Dobson circulation, *Climate Dynamics*, 27, 727–741,
 471 <https://doi.org/10.1007/s00382-006-0162-4>, 2006.
- 472 Butchart, N., Anstey, J., Hamilton, K., Osprey, S., McLandress, C., Bushell, A. C., Kawatani, Y., Kim,
 473 Y.-H., Lott, F., Scinocca, J., Stockdale, T.N., Andrews, M., Bellprat, O., Braesicke, P., Cagnazzo,
 474 C., Chen, C.-C., Chun, H.-Y., Dobrynin, M., Garcia, R., Garcia-Serrano, J., Gray, L.J., Holt, L.,
 475 Kerzenmacher, T., Naoe, H., Pohlmann, H., Richter, J. H., Scaife, A.A., Schenzinger, V., Serva, F.,
 476 Versick, S., Watanabe, S., Yoshida, K. and Yukimoto, S.: Overview of experiment design and
 477 comparison of models participating in phase 1 of the SPARC Quasi-Biennial Oscillation initiative
 478 (QBOi), *Geoscientific Model Development*, 11, 1009–1032. [https://doi.org/10.5194/gmd-11-1009-](https://doi.org/10.5194/gmd-11-1009-2018)
 479 [2018](https://doi.org/10.5194/gmd-11-1009-2018), 2018.
- 480 Butchart, N., Anstey, J. A., Kawatani, Y., Osprey, S. M., Richter, J. H., Wu, T.: QBO changes in CMIP6
 481 climate projections, *Geophys. Res. Lett.*, 47, 1–10. <https://doi.org/10.1029/2019GL086903>, 2020.

482 Camargo, S. J. and Sobel, A. H.: Revisiting the influence of the quasi-biennial oscillation on tropical
 483 cyclone activity, *J. Climate*, 23, 5810–5825, <https://doi.org/10.1175%2F2010JCLI3575.1>, 2010.
 484 Collimore, C. C., Martin, D. W., Hitchman, M. H., Huesmann, A., and Waliser, D. E.: On the
 485 relationship between the QBO and tropical deep convection, *J. Climate*, 16, 2552–2568,
 486 [https://doi.org/10.1175/1520-0442\(2003\)016%3C2552:OTRBTQ%3E2.0.CO;2](https://doi.org/10.1175/1520-0442(2003)016%3C2552:OTRBTQ%3E2.0.CO;2), 2003.
 487 Dickinson, R. E.: Method of parameterization for infrared cooling between altitudes of 30 and 70
 488 kilometers, *J. Geophys. Res.*, 78, 4451–4457, <https://doi.org/10.1029/JC078i021p04451>, 1973.
 489 Dunkerton, T. J.: The role of gravity waves in the quasi-biennial oscillation, *J. Geophys. Res.*, 102,
 490 26053–26076, <https://doi.org/10.1029/96JD02999>, 1997.
 491 Ebdon, R. A.: Notes on the wind flow at 50mb in tropical and subtropical regions in January 1957 and in
 492 1958, *Q. J. Roy. Meteor. Soc.*, 86, 540–542, <https://doi.org/10.1002/qj.49708637011>, 1960.
 493 Eichinger, R. and Šácha, P.: Overestimated acceleration of the advective Brewer-Dobson circulation due
 494 to stratospheric cooling, *Q. J. R. Meteorol. Soc.*, 1-15, <https://doi.org/10.1002/qj.3876>, 2020.
 495 Fels, S. B.: A parameterization of scale-dependent radiative damping rates in the middle atmosphere, *J.*
 496 *Atmos. Sci.*, 39, 1141–1152, [https://doi.org/10.1175/1520-](https://doi.org/10.1175/1520-0469(1982)039%3C1141:APOSDR%3E2.0.CO;2)
 497 [0469\(1982\)039%3C1141:APOSDR%3E2.0.CO;2](https://doi.org/10.1175/1520-0469(1982)039%3C1141:APOSDR%3E2.0.CO;2), 1982.
 498 Fels, S. B.: Radiative-dynamical interactions in the middle atmosphere, *Advances in Geophysics*, Vol.
 499 28A, Academic Press, 277–300, [https://doi.org/10.1016/S0065-2687\(08\)60227-7](https://doi.org/10.1016/S0065-2687(08)60227-7), 1985.
 500 Garfinkel, C. I. and Hartmann, D. L.: The influence of the quasi-biennial oscillation on the troposphere
 501 in winter in a hierarchy of models. Part I: Simplified dry GCMs, *J. Atmos. Sci.*, 68, 1273–1289,
 502 <https://doi.org/10.1175%2F2011JAS3665.1>, 2011a.

503 Garfinkel, C. I. and Hartmann, D. L.: The influence of the quasi-biennial oscillation on the troposphere
 504 in winter in a hierarchy of models. Part II: Perpetual winter WACCM runs, *J. Atmos. Sci.*, 68, 2026–
 505 2041, <https://doi.org/10.1175%2F2011JAS3702.1>, 2011b.

506 Geller, M. A., Zhou, T., Shindell, D., Ruedy, R., Aleinov, I., Nazarenko, L., Tausnev, N. L., Kelley, M.,
 507 Sun, S., Cheng, Y., Field, R. D., and Faluvegi, G.: Modeling the QBO-improvements resulting from
 508 higher-model vertical resolution, *J. Adv. Model. Earth Syst.*, 8, 1092–1105,
 509 <https://doi.org/10.1002/2016MS000699>, 2016a.

510 Geller, M. A., Zhou, T., and Yuan, W.: The QBO, gravity waves forced by tropical convection, and
 511 ENSO, *J. Geophys. Res. Atmos.*, 121, 8886–8895, <https://doi.org/10.1002/2015JD024125>, 2016b.

512 Gidden, M. J., Riahi, K., Smith, S. J., Fujimori, S., Luderer, G., Kriegler, E., van Vuuren, D. P., van den
 513 Berg, M., Feng, L., Klein, D., Calvin, K., Doelman, J. C., Frank, S., Fricko, O., Harmsen, M.,
 514 Hasegawa, T., Havlik, P., Hilaire, J., Hoesly, R., Horing, J., Popp, A., Stehfest, E., and Takahashi,
 515 K.: Global emissions pathways under different socioeconomic scenarios for use in CMIP6: a dataset
 516 of harmonized emissions trajectories through the end of the century, *Geosci. Model Dev.*, 12, 1443–
 517 1475, <https://doi.org/10.5194/gmd-12-1443-2019>, 2019.

518 Giorgetta, M. A. and Doege, M. C.: Sensitivity of the Quasi-Biennial Oscillation to CO₂ doubling,
 519 *Geophys. Res. Lett.*, 32, L08701. <https://doi.org/10.1029/2004GL021971>, 2005.

520 Giorgetta, M. A., Bengtson, L., and Arpe, K.: An investigation of QBO signals in the east Asian and
 521 Indian monsoon in GCM experiments, *Climate Dynamics*, 15, 435–450,
 522 <https://doi.org/10.1007/s003820050292>, 1999.

523 Giorgetta, M. A., Manzini, E., and Roeckner, E.: Forcing of the quasi-biennial oscillation from a broad
 524 spectrum of atmospheric waves, *Geophys. Res. Lett.*, 29, <https://doi.org/10.1029/2002GL014756>,
 525 2002.

526 Giorgetta, M. A., Manzini, E., Roeckner, E., Esch, M., and Bengtsson, L.: Climatology and forcing
 527 of the quasi-biennial oscillation in the MAECHM5 model, *J. Climate*, 19, 3882–3901,
 528 <https://doi.org/10.1175/JCLI3830.1>, 2006.

529 Gray, W. M.: Atlantic seasonal hurricane frequency. Part I: El Niño and 30-mb quasi-biennial oscillation
 530 influences, *Mon. Wea. Rev.*, 112, 1649–1688, [https://doi.org/10.1175/1520-0493\(1984\)112%3C1649:ASHFPI%3E2.0.CO;2](https://doi.org/10.1175/1520-0493(1984)112%3C1649:ASHFPI%3E2.0.CO;2), 1984.

532 Gray, W. M., Sheaffer, J. D., and Knaff, J.: Influence of the stratospheric QBO on ENSO variability, *J.*
 533 *Meteor. Soc. Jpn.*, 70, 975–995, https://doi.org/10.2151/jmsj1965.70.5_975, 1992.

534 Hamilton, K.: The vertical structure of the quasi-biennial oscillation: Observations and theory, *Atmos.*
 535 *Ocean*, 19, 236–250, <http://dx.doi.org/10.1080/07055900.1981.9649111>, 1981.

536 Hansen, F., Matthes, K., and Wahl, S.: Tropospheric QBO–ENSO interactions and differences between
 537 the Atlantic and Pacific, *J. Climate*, 29, 1353–1368, <https://doi.org/10.1175/JCLI-D-15-0164.1>,
 538 2016

539 Hasebe, F.: Quasi-biennial oscillations of ozone and diabatic circulation in the equatorial stratosphere, *J.*
 540 *Atmos. Sci.*, 51, 729–745, [https://doi.org/10.1175/1520-0469\(1994\)051%3c0729:QBOOOA%3e2.0.CO;2](https://doi.org/10.1175/1520-0469(1994)051%3c0729:QBOOOA%3e2.0.CO;2), 1994.

542 Hitchman, M. H., and Huesmann, A. S.: Seasonal influence of the quasi-biennial oscillation on
 543 stratospheric jets and Rossby wave breaking, *J. Atmos. Sci.*, 66, 935–946,
 544 <https://doi.org/10.1175%2F2008JAS2631.1>, 2009.

545 Ho, C.-H., Kim, H.-S., Jeong, J.-H., and Son, S.-W.: Influence of stratospheric quasi-biennial oscillation
 546 on tropical cyclone tracks in the western North Pacific, *Geophys. Res. Lett.*, 36, L06702,
 547 <http://dx.doi.org/10.1029/2009GL037163>, 2009.

548 Holt, L., Lott, F., Garcia, R., Kiladis, G.N., Anstey, J.A., Braesicke, P., Bushell, A.C., Butchart, N.,
 549 Cagnazzo, C., Chen, C.-C., Chun, H.-Y., Hamilton, K., Kawatani, Y., Kerzenmacher, T., Kim, Y.-
 550 H., McLandress, C., Naoe, H., Osprey, S., Richter, J.H., Scinocca, J., Serva, F., Versick, S.,
 551 Watanabe, S., Yoshida, K., and Yukimoto, S.: An evaluation of tropical waves and wave forcing of
 552 the QBO in the QBOi models, Q. J. R. Meteorol. Soc., <https://doi.org/10.1002/qj.3827>, 2020.
 553 Holton, J. R. and Lindzen, R. S.: An updated theory for the quasi-biennial cycle of the tropical
 554 stratosphere, J. Atmos. Sci., 29, 1076–1080, [https://doi.org/10.1175/1520-0469\(1972\)029%3c1076:AUTFTQ%3e2.0.CO;2](https://doi.org/10.1175/1520-0469(1972)029%3c1076:AUTFTQ%3e2.0.CO;2), 1972.
 555
 556 Holton, J. R. and Tan, H.: The Influence of the equatorial quasi-biennial oscillation on the global
 557 circulation at 50 mb, J. Atmos. Sci., 37, 2200–2208, [https://doi.org/10.1175/1520-0469\(1980\)037%3c2200:TIOTEQ%3e2.0.CO;2](https://doi.org/10.1175/1520-0469(1980)037%3c2200:TIOTEQ%3e2.0.CO;2), 1980.
 558
 559 Huang, B. H., Hu, Z. Z., Kinter, J. L., Wu, Z. H., and Kumar, A.: Connection of stratospheric QBO with
 560 global atmospheric general circulation and tropical SST. Part I: Methodology and composite life
 561 cycle, Climate Dynamics, 38, 1–23, <https://doi.org/10.1007%2Fs00382-011-1250-7>, 2012.
 562 Kawatani, Y. and Hamilton, K.: Weakened stratospheric Quasi-Biennial Oscillation driven by increased
 563 tropical mean upwelling, Nature, 497, 478–481, <https://doi.org/10.1038/nature12140>, 2013.
 564 Kawatani, Y., Takahashi, M., Sato, K., Alexander, S. P., and Tsuda, T.: Global distribution of
 565 atmospheric waves in the equatorial upper troposphere and lower stratosphere: AGCM simulation
 566 of sources and propagation, J. Geophys. Res., 114, D01102, <https://doi.org/10.1029/2008JD010374>,
 567 2009.
 568 Kawatani, Y., Watanabe, S., Sato, K., Dunkerton, T. J., Miyahara, S., and Takahashi, M.: The roles of
 569 equatorial trapped waves and internal inertia-gravity waves in driving the Quasi-Biennial oscillation.

570 Part I: Zonal mean wave forcing, *J. Atmos. Sci.*, 67, 963–980,
 571 <https://doi.org/10.1175/2009JAS3222.1>, 2010.
 572 Kawatani, Y., Hamilton, K., and Watanabe, S.: The quasi-biennial oscillation in a double CO₂ climate,
 573 *J. Atmos. Sci.*, 68, 265–283, <https://doi.org/10.1175/2010JAS3623.1>, 2011.
 574 Kawatani, Y., Lee, J. N., and Hamilton, K.: Interannual variations of stratospheric water vapor in MLS
 575 observations and climate model simulations, *J. Atmos. Sci.*, 71, 4072–4085,
 576 <https://doi.org/10.1175/JAS-D-14-0164.1>, 2014.
 577 Kawatani, Y., Hamilton, K., Sato, K., Dunkerton, T. J., Watanabe, S., and Kikuchi, K.: ENSO Modulation
 578 of the QBO: Results from MIROC Models with and without Nonorographic Gravity Wave
 579 Parameterization, *J. Atmos. Sci.*, 76, 3893–3917, <https://doi.org/10.1175/JAS-D-19-0163.1>, 2019.
 580 Labitzke, K.: On the interannual variability of the middle stratosphere during the northern winters, *J.*
 581 *Meteorol. Soc. Jpn.*, 80, 963–971, http://doi.org/10.2151/jmsj1965.60.1_124, 1982.
 582 Lait, L. R., Schoeberl, M. R., and Newman, P. A.: Quasi-biennial modulation of the Antarctic ozone
 583 depletion, *J. Geophys. Res.*, 94, 11559–11571, <http://dx.doi.org/10.1029/JD094iD09p11559>, 1989.
 584 Li, F., Austin, J., and Wilson, R. J.: The strength of the Brewer–Dobson circulation in a changing climate:
 585 Coupled chemistry–climate model simulations, *J. Climate*, 21, 40–57,
 586 <https://doi.org/10.1175/2007JCLI1663.1>, 2008.
 587 Liess, S. and Geller, M. A.: On the relationship between QBO and distribution of tropical deep
 588 convection, *J. Geophys. Res.*, 117, D03108, <http://dx.doi.org/10.1029/2011JD016317>, 2012.
 589 Lindzen, R. S.: Equatorial planetary waves in shear: Part I, *J. Atmos. Sci.* 28, 609–622,
 590 [https://doi.org/10.1175/1520-0469\(1971\)028%3C0609:EPWISP%3E2.0.CO;2](https://doi.org/10.1175/1520-0469(1971)028%3C0609:EPWISP%3E2.0.CO;2), 1971.
 591 Lindzen, R. S. and Holton, J. R.: A theory of the quasi-biennial oscillation, *J. Atmos. Sci.*, 25, 1095–
 592 1107, [https://doi.org/10.1175/1520-0469\(1968\)025%3C1095:ATOTQB%3E2.0.CO;2](https://doi.org/10.1175/1520-0469(1968)025%3C1095:ATOTQB%3E2.0.CO;2), 1968.

593 Marshall, A. G. and Scaife, A. A.: Impact of the QBO on surface winter climate, *J. Geophys. Res.*, 114,
 594 D18110, <http://dx.doi.org/10.1029/2009JD011737>, 2009.

595 Match, A., and Fueglistaler, S.: The buffer zone of the quasi-biennial oscillation, *J. Atmos. Sci.*, 76, 3553–
 596 3567, <https://doi.org/10.1175/JAS-D-19-0151.1>, 2019

597 Match, A., and Fueglistaler, S.: Mean-flow damping forms the buffer zone of the quasi-biennial
 598 oscillation: 1D theory. *J. Atmos. Sci.*, 77, 1955–1967, <https://doi.org/10.1175/JAS-D-19-0293.1>,
 599 2020.

600 Matsuno, T.: Numerical integrations of primitive equations by use of a simulated backward difference
 601 method, *J. Meteor. Soc. Japan*, 44, 76–84, https://doi.org/10.2151/jmsj1965.44.1_76, 1966

602 Plass, G. N.: The influence of the 15 μ carbon-dioxide band on the atmospheric infra-red cooling rate,
 603 *Quart. J. Roy. Meteor. Soc.*, 82, 310–324, <https://doi.org/10.1002/qj.49708235307>, 1956.

604 Plumb, R. A.: The interaction of two internal waves with the mean flow: Implications for the theory of
 605 the quasi-biennial oscillation, *J. Atmos. Sci.*, 34, 1847–1858, [https://doi.org/10.1175/1520-0469\(1977\)034<1847:TIOTIW>2.0.CO;2](https://doi.org/10.1175/1520-0469(1977)034<1847:TIOTIW>2.0.CO;2), 1977.

607 Reed, R. J., Campbell, W. J., Rasmussen, L. A., and Rogers, D. G.: Evidence of a downward-propagating,
 608 annual wind reversal in the equatorial stratosphere, *J. Geophys. Res.*, 66, 813–818,
 609 <http://dx.doi.org/10.1029/JZ066i003p00813>, 1961.

610 Richter, J. H., Anstey, J. A., Butchart, N., Kawatani, Y., Meehl, G. A., Osprey, S., & Simpson, I. R.,
 611 2020b: Progress in simulating the quasi-biennial oscillation in CMIP models. *Journal Geophysical*
 612 *Research: Atmospheres*, 125, e2019JD032362, <https://doi.org/10.1029/2019JD032362>, 2020a.

613 Richter, J. H., Butchart, N., Kawatani, Y., Bushell, A. C., Holt, L., Serva, F., Anstey, J., Simpson, I. R.,
 614 Osprey, S., Hamilton, K., Braesicke, P., Cagnazzo, C., Chen, C.-C., Garcia, R. R., Gray, L. J.,
 615 Kerzenmacher, T., Lott, F., McLandress, C., Naoe, H., Scinocca, J., Stockdale, T. N., Versick, S.,

616 Watanabe, S., Yoshida, K., Yukimoto, S.: Response of the Quasi-Biennial Oscillation to a warming
 617 climate in global climate models, Q. J. R. Meteorol. Soc., 1–29, <https://doi.org/10.1002/qj.3749>,
 618 2020b.

619 Rind, D., Jonas, J., Balachandran, N., Schmidt, G., and Lean, J.: The QBO in two GISS global climate
 620 models: 1. Generation of the QBO, J. Geophys. Res. Atmos., 119, 8798–8824,
 621 <https://doi.org/10.1002/2014JD021678>, 2014.

622 Rind, D., Orbe, C., Jonas, J., Nazarenko, L., Zhou, T., Kelley, M., Lacis, A., Shindell, D., Faluvegi,
 623 Russell, G., Bauer, M., Schmidt, G., Romanou, A., and Tausnev, N.: GISS Model E2.2: A climate
 624 model optimized for the middle atmosphere — Model structure, climatology, variability and climate
 625 sensitivity, J. Geophys. Res. Atmos., 125, e2019JD032204, <https://doi.org/10.1029/2019JD032204>,
 626 2020.

627 Saravanan, R.: A multiwave model of the quasi-biennial oscillation, J. Atmos. Sci., 47, 2465–2474,
 628 [https://doi.org/10.1175/1520-0469\(1990\)047%3C2465:AMMOTQ%3E2.0.CO;2](https://doi.org/10.1175/1520-0469(1990)047%3C2465:AMMOTQ%3E2.0.CO;2), 1990.

629 Scaife, A. A., Butchart, N., Warner, C. D., Stainforth, D., Norton, W., and Austin, J.: Realistic quasi-
 630 biennial oscillations in a simulation of the global climate, Geophys. Res. Lett., 27, 3481–3484,
 631 <https://doi.org/10.1029/2000GL011625>, 2000.

632 Schirber, S., Manzini, E., Krismer, T. and Giorgetta, M.: The Quasi-Biennial Oscillation in a warmer
 633 climate: sensitivity to different gravity wave parameterizations, Climate Dynamics, 45, 825–
 634 836, <https://doi.org/10.1007/s00382-014-2314-2>, 2015.

635 Trepte, C. R. and Hitchman, M. H.: Tropical stratospheric circulation deduced from satellite aerosol data,
 636 Nature, 355, 626–628, <https://doi.org/10.1038/355626a0>, 1992.

637 Watanabe, S. and Kawatani, Y.: Sensitivity of the QBO to mean tropical upwelling under a changing
638 climate simulated with an Earth System Model, Journal of the Meteorological Society of Japan,
639 Series II, 90A, 351–360, <https://doi.org/10.2151/jmsj.2012-A20>, 2012.

640 Yoo, C. and Son, S.-W.: Modulation of the boreal wintertime Madden-Julian oscillation by the
641 stratospheric quasi-biennial oscillation, Geophys. Res. Lett., 43, 1392–1398,
642 <https://doi.org/10.1002%2F2016GL067762>, 2016.

643 Zawodny, J. M. and McCormick, M. P.: Stratospheric Aerosol and Gas Experiment II measurements of
644 the quasi-biennial oscillations in ozone and nitrogen dioxide, J. Geophys. Res., 96, 9371– 9377,
645 <http://dx.doi.org/10.1029/91JD00517>, 1991.

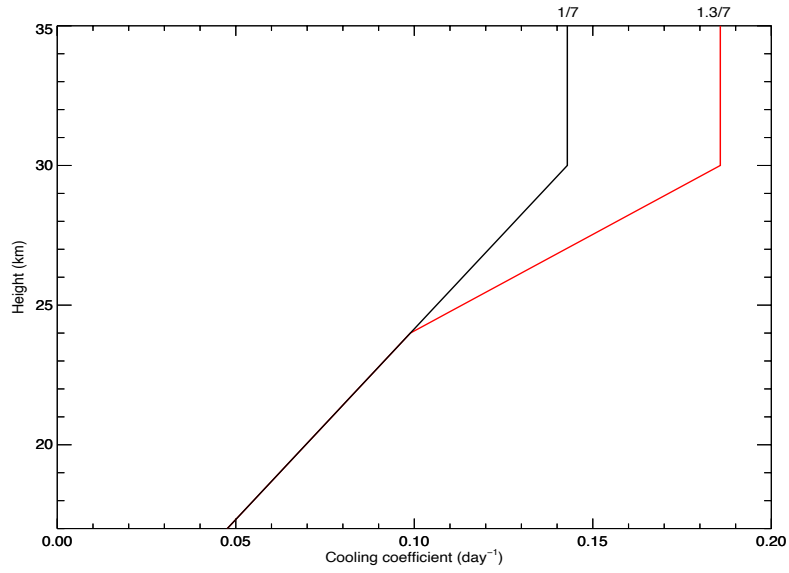


FIG. 1: Newtonian cooling profiles: The smaller values (black line) are used for the control runs while the larger values (red line) are used for the experimental runs.

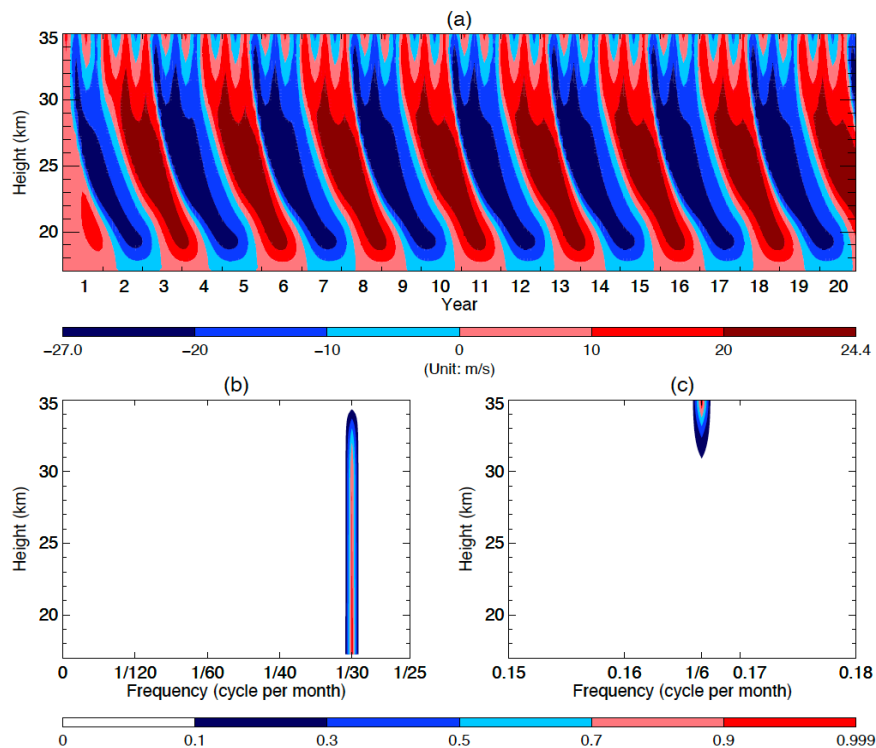


FIG. 2: (a) Time–height section of the monthly averaged mean zonal wind over the first 20 years from the HL’s original model. (b) and (c) Frequency–height section of the power spectral densities (PSD) of the standardized monthly averaged mean zonal wind of the 100 years. Note that in order to better visualize the PSD in (b) and (c), we trimmed off the blank segments for the frequencies ranging from $\frac{1}{25}$ to 0.15 cycle per month and those ranging from 0.18 to 0.5 cycle per month.

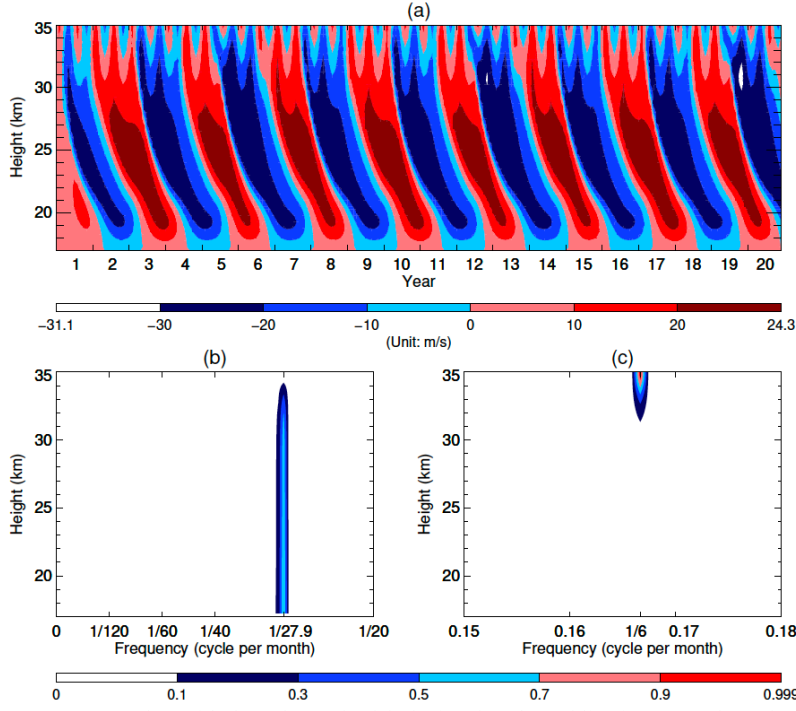


FIG. 3: (a) Same as FIG. 2a, but with the enhanced $\alpha(z)$ depicted as the red line in FIG. 1. (b) and (c) Frequency–height section of the power spectral densities (PSD) of the standardized monthly averaged mean zonal wind of the 100 years. Note that in order to better visualize the PSD in (b) and (c), we trimmed off the blank segments for the frequencies ranging from $\frac{1}{20}$ to 0.15 cycle per month and those ranging from 0.18 to 0.5 cycle per month.

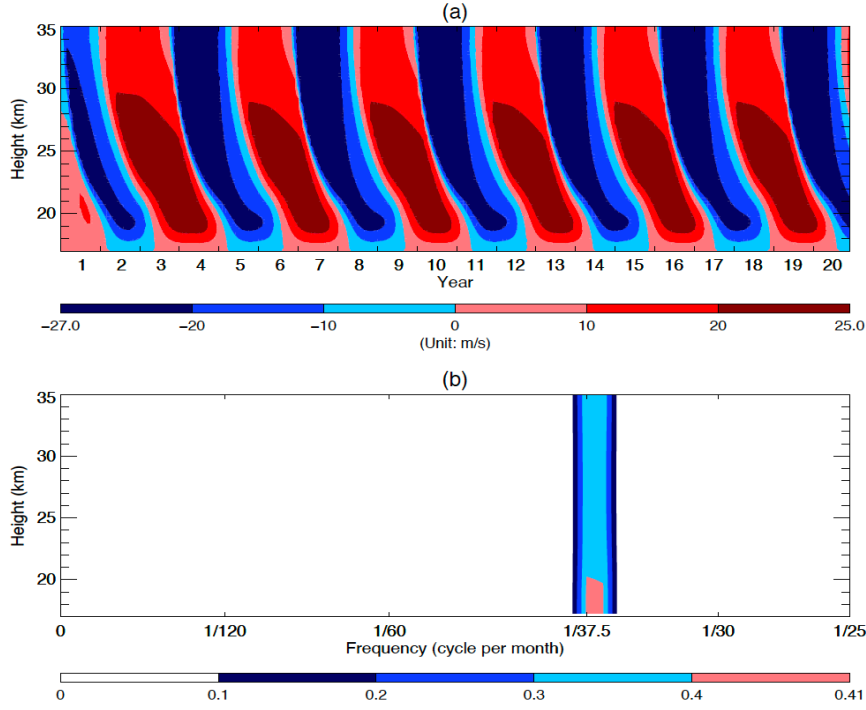


FIG. 4: (a) Time–height section of the monthly averaged mean zonal wind over the first 20 years from the HL’s model without the semiannual forcing. (b) Frequency–height section of the power spectral densities (PSD) of the standardized monthly averaged mean zonal wind of the 100 years. Note that in order to visualize the PSD, we trimmed off the blank segment for the frequencies ranging from $\frac{1}{25}$ to 0.5 cycle per month.

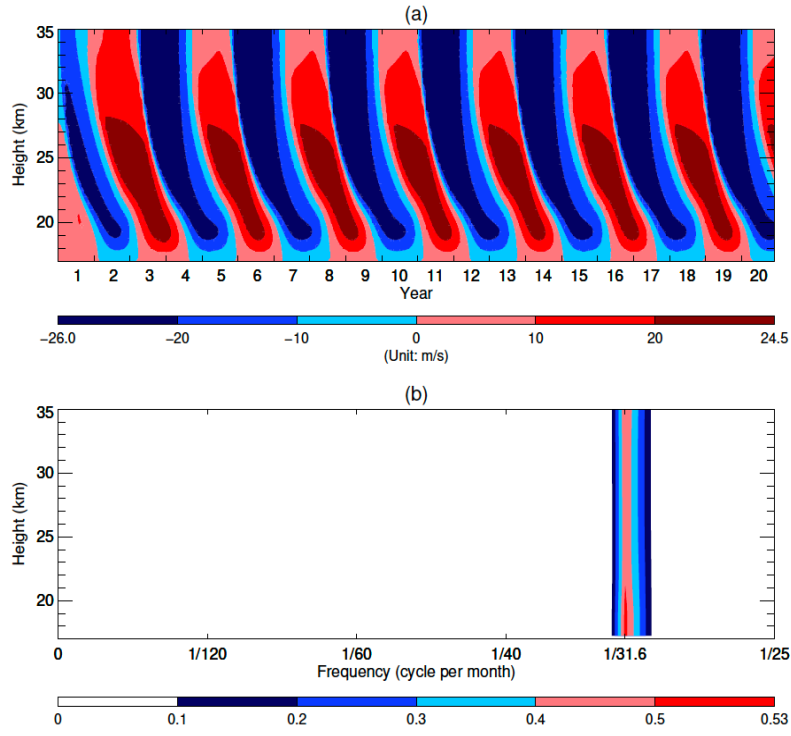


FIG. 5: (a) Same as FIG. 4a, but with the enhanced $\alpha(z)$ depicted as the red line in FIG. 1. (b) Same as FIG. 4b, but for the doubled CO₂ Run.

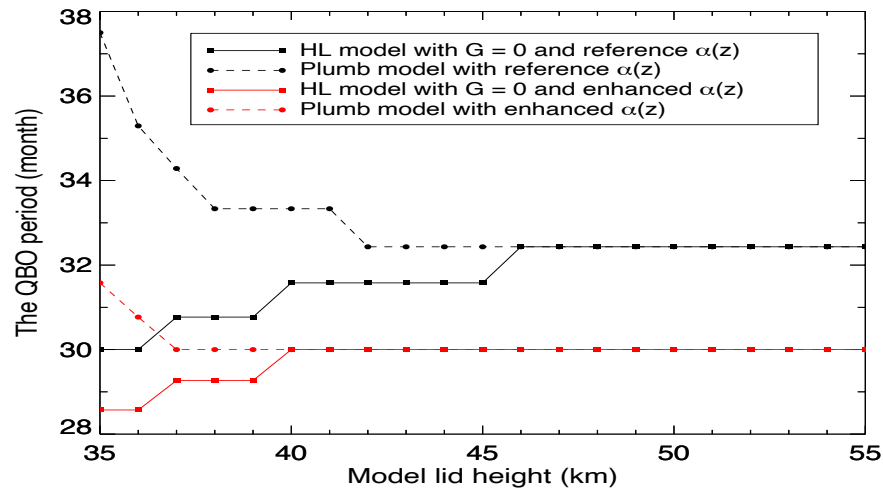


FIG. 6: The relationship between the simulated QBO period with the height of the model lid. Black and red lines depict the results from using the reference radiative damping and the enhanced radiative damping respectively while solid and dashed lines delineate the results from the HL model with $G = 0$ and the Plumb model respectively.